

An Experimental Study of the Stability and Dynamics of Langmuir Films of Fullerene Derivatives and Their Mixtures with Pentadecanoic Acid

Maria-Paula Hernández, Francisco Monroy,* Francisco Ortega, and Ramón G. Rubio

Departamento de Química Física I, Facultad de Ciencias Químicas, Universidad Complutense, E-28040 Madrid, Spain

Ángel Martín-Domenech, Eva M^a Priego, Luis Sánchez, and Nazario Martín

Departamento de Química Orgánica I, Facultad de Ciencias Químicas, Universidad Complutense, E-28040 Madrid, Spain

Received October 23, 2000. In Final Form: February 1, 2001

The synthesis and behavior of the Langmuir monolayers of several fullerene (C₆₀) derivatives is reported. True monolayers are found only for one derivative with a 12 C-atom chain substituent. The interfacial rheology of these monolayers has been studied by measuring the thermal capillary wave spectra. It is found that the elasticity and the dilational viscosity increase from diluted monolayers to an area per molecule of approximately 150 Å², which roughly corresponds to the equilibrium distance for the intermolecular potential of the fullerene molecules. For more compressed monolayers both the elasticity and viscosity decrease. These results can be qualitatively explained in terms of the model described by Evans for monolayers of C₆₀ (Evans, A. K. *J. Phys. Chem.* **1998**, *102*, 7016). The mixed Langmuir monolayers of *x* pentadecanoic acid + (1 - *x*) fullerene derivative have also been studied, for 0 ≤ *x* ≤ 1. True monolayers are found up to high values of *x*. The monolayers present a liquid expanded to liquid condensed transition up to values of *x* corresponding to one fullerene molecule per six of acid. This can be interpreted in terms of the ability of the mixture to maintain the hexagonal structure characteristic of the monolayer of pure pentadecanoic acid.

1. Introduction

Ordered molecular films, with thickness ranging from a few nanometers in the case of a monolayer to several hundred nanometers, show considerable technological promise. In fact, as a consequence of the miniaturizing effort in the microelectronic industry, self-assembled organic films have been proposed as satisfactory candidates to replace both passive and active components commonly used in electronic and optical devices. The study of the molecular interactions in thin-film structures is a necessary step for a better understanding of the collective properties of the ordered arrays of conducting or semiconducting materials incorporated in these useful devices.

Fullerene and its derivatives have generated a lot of scientific research since its discovery by Kroto et al.¹ 15 years ago. The particular physicochemical properties of fullerenes, essentially due to their singular geometry and electronic structure, have become the focus of considerable interest in monomeric or aggregated forms. Fullerene-based materials show superconductivity,² photoconductivity,³ and nonlinear optical behavior.⁴ Some interesting and promising pharmacological properties of fullerenes have been also reported, e.g., as enzymatic inhibitor of the HIV-protease⁵ or as trans-membrane charge transfer.⁶

Numerous efforts have been devoted to the elaboration of well-ordered monomolecular films of fullerenes since their electronic properties may be better controlled in a bidimensional arrangement.^{7–9} Although from measurements of Π–*A* isotherms, Obeng and Bard reported for the first time the formation of a stable monolayer of fullerene (C₆₀) at the air–water interface⁷ (the precursor for Langmuir–Blodgett (LB) production), many studies have revealed afterward that, under the most common experimental conditions, C₆₀ does not form truly stable monolayers.^{8,10–12}

A recent Langevin dynamics simulation provided a clear explanation for the strong tendency of C₆₀ molecules to form three-dimensional aggregates when spread onto the water surface.¹³ The so-formed multilayer arrangements have been experimentally confirmed by UV–vis spectroscopy (band centered at 450 nm).¹⁴ The aggregation explains the fact that experimental Π–*A* isotherms of C₆₀

(1) Kroto, H. W.; Heath, J. R.; O'Brien, S. C.; Curl, R. F.; Smalley, R. E. *Nature* **1985**, *318*, 162.

(2) Hebard, A. F.; Rosseinsky, M. J.; Haddon, R. C.; Murphy, D. W.; Glarum, S. H.; Palstra, T. T.; Ramirez, A. T.; Kortan, A. R. *Nature* **1991**, *350*, 600.

(3) Minami, M. *Chem. Lett.* **1991**, *10*, 1791.

(4) Wang, X. K.; Zhang, T. G.; Lin, W. P.; Sheng, Z. L.; Wong, G.; Kappes, M. M.; Chang, R. P. H.; Ketterson, J. B. *Appl. Phys. Lett.* **1992**, *60*, 810.

(5) Friedman, S. H.; De Camp, D. L.; Sijbesma, R. P.; Srdanov, G.; Wuld, F.; Kenyon, G. L. *J. Am. Chem. Soc.* **1993**, *115*, 6506.

(6) Li, D. Q.; Swanson, B. I. *Langmuir* **1993**, *9*, 3341. For a recent review on medical applications of fullerenes, see: Prato, M.; Da Ros, T. *Chem. Commun.* **1999**, 663.

(7) Obeng, Y. S.; Bard, A. J. *J. Am. Chem. Soc.* **1991**, *113*, 6279.

(8) Milliken, J.; Dominguez, D. D.; Nelson, H. H.; Barger, W. R. *Chem. Mater.* **1992**, *4*, 252.

(9) Brousseau, J. L.; Tian, K.; Gauvin, S.; Leblanc, R. M.; Delhaès, P. *Chem. Phys. Lett.* **1993**, *202*, 521.

(10) Maliszewskyj, N. C.; Heiney, P. A.; Jones, D. R.; Strongin, R. M.; Cichy, M. A.; Smith, A. B. *Langmuir* **1993**, *9*, 1439.

(11) Back, R.; Lennox, R. B. *J. Phys. Chem.* **1992**, *96*, 8149.

(12) Castillo, R.; Ramos, S.; Ruiz-García, J. *J. Phys. Chem.* **1996**, *100*, 15235.

(13) Evans, A. K. *J. Phys. Chem.* **1998**, *102*, 7016.

(14) Ravaine, S.; Mingotaud, C.; Delhaès, P. *Thin Solid Films* **1996**, *284*, 76.

usually lead to values for the limiting surface area much lower than the one expected for a spherical molecule with cross-sectional area ca. 87 \AA^2 . Moreover, A_0 is strongly dependent on the experimental protocol followed for spreading C_{60} at the air–water interface.

Two strategies are usually followed in order to avoid the aggregation process mentioned above: the first one is to functionalize the C_{60} moiety by attaching a polar group, thus obtaining molecules with amphiphilic character;^{14–17} a second way is to mix C_{60} with a good film-forming agent. These two alternative routes have been followed in this work: first, we will carry out a thermodynamic study of pure films of three new C_{60} functionalized derivatives. Second, we will study the interfacial compatibility of C_{60} , and some of the derivatives studied with pentadecanoic acid (PDA), which is well-known to form stable Langmuir monolayers at the air–water interface. The stability and compatibility of this bidimensional blend will be studied from the behavior of the Π – A isotherms as a function of composition, of surface concentration, and, in some cases, of temperature.

Recent surface-force measurements have suggested that C_{60} molecules exhibit surprising tribological properties in confined geometries.^{18,19} It has been argued that free rotation of these spherical molecules when confined in the vicinity of the solid–liquid interface should be in the molecular basis for the abnormally small values of the shear viscosity reported when increasing confinement.

Surface quasi-elastic light scattering (SQELS) has long been used as a probe of the dynamics of films at fluid interfaces.²⁰ The light scattered at wavevector q by thermally excited capillary modes of a film spread at the air–water interface is primarily governed by surface tension, γ , $I_{\text{scatt}} \sim k_B T \gamma q^2$. The analysis of the power spectrum of the light scattered, $P_q(\omega)$, can be done in terms of the elasto-hydrodynamic theory initially developed by Kramer²¹ and Bouchiat et al.²² and provides the complex viscoelastic modulus of the film, $\tilde{\epsilon}(\omega) = \epsilon + i\omega\kappa$, ϵ and κ being the dilational elasticity and viscosity, respectively, both containing hydrostatic compression and shear components, i.e., $\tilde{\epsilon}(\omega) = \tilde{\epsilon}_C(\omega) + \tilde{\epsilon}_S(\omega)$.^{20,23,24}

$$P_q(\omega) = -\frac{2k_B T}{\omega} \text{Im}\{[\tilde{\epsilon}q^2 + i\omega\eta(q+m)] / [\gamma q^2 + i\omega\eta(q+m) - \rho\omega^2/q][\tilde{\epsilon}q^2 + i\omega\eta(q+m)] + [\omega\eta(q-m)^2]\} \quad (1)$$

with $m^2 = q^2 + i\omega\rho/\eta$, being ρ and η , respectively, the density and viscosity of water; ω and q are the frequency and wavevector of the capillary mode, respectively.

To explore the high-frequency dynamics and to check for viscoelastic relaxations on a true 2D arrangement of

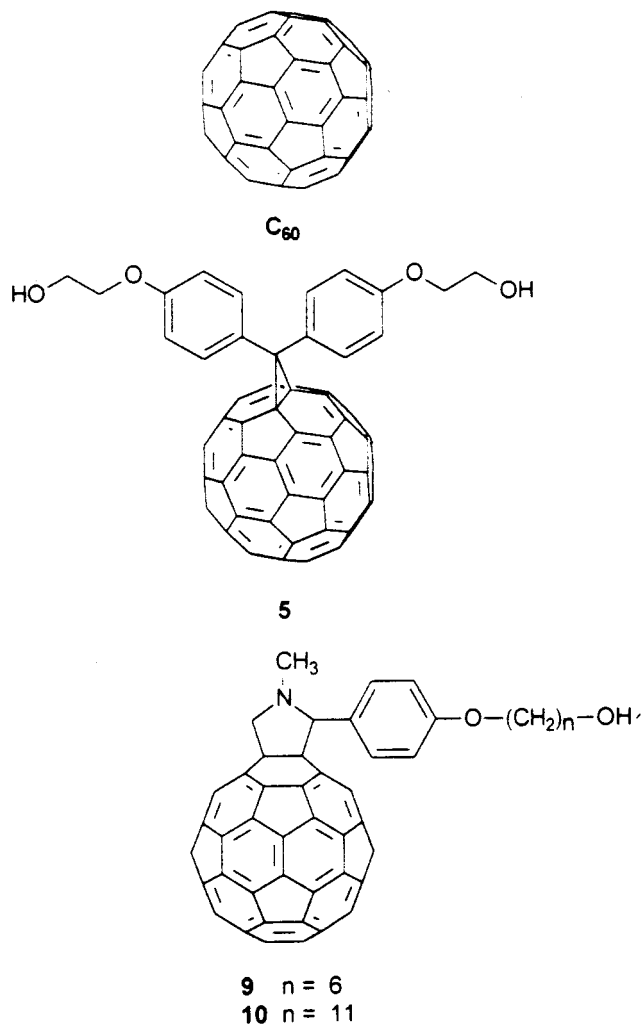


Figure 1. Chemical structures of pure C_{60} and the functionalized derivatives **5**, **9**, and **10**.

these spherical weakly interacting molecules, we shall study by SQELS well-formed and stable monolayers of fullerene derivatives at the air–water interface. The results will be discussed in terms of some of the predictions of Evans¹³ for dynamics of fullerenes at the air–water interface.

The rest of this paper will be organized as follows. The synthesis and characterization methods of the chemicals and the experimental details are summarized in section 2. The experimental results and its discussion are presented in section 3. Finally, the main conclusions are given in section 4.

2. Materials and Methods

2.a. Chemicals. C_{60} was purchased from MER Corporation (95%) and used as received without further purification. We have also studied the three different functionalized derivatives of C_{60} in Figure 1, which have been synthesized according to the procedures described below. The OH-ended functional groups grafted to the C_{60} molecule have been chosen to be, when pure, sufficiently polar to form stable monolayers at the air–water interface. Compound **5** has two small alkyl chains, while only one, much longer, has been attached to derivatives **9** and **10**.

We used benzene (Carlo Erba, RPE grade) as spreading solvent. The benzene solutions of C_{60} and its derivatives (ca. 0.1 mM) were stored at 2 °C between experiments to limit solvent evaporation. Pentadecanoic acid, PDA (Fluka), with a purity of +99.9% was used as received. The subphase, acidified at pH = 2 to prevent for PDA hydrolysis, was obtained by adding a HCl solution (Carlo Erba). The water used for subphase preparation

(15) Maggini, M.; Pasimeni, L.; Prato, M.; Scorrano, G.; Valli, L. *Langmuir* **1994**, *10*, 4164.

(16) Matsumoto, M.; Tachibana, H.; Azumi, R.; Tanaka, M.; Nakamura, T.; Yunome, G.; Abe, M.; Yabago, S.; Nakamura, E. *Langmuir* **1995**, *11*, 660.

(17) Ravaine, S.; Mingotaud, C.; Delhaès, P. *Synth. Met.* **1996**, *284*, 76.

(18) Campbell, S. E.; Luengo, G.; Srdanov, V. I.; Wudl, F.; Israelachvili, J. N.; *Nature* **1996**, *382*, 520; Luengo, G.; Campbell, S. E.; Srdanov, V. I.; Wudl, F.; Israelachvili, J. N. *Chem. Mater.* **1997**, *9*, 1166.

(19) Zhao, W.; Tang, J.; Puri, A.; Sweany, R. L.; Li, Y. L.; Chen, L. *J. Mater. Res.* **1996**, *11*, 2749.

(20) Langevin, D. *Light Scattering by Liquid Surfaces and Complementary Techniques*; Dekker: New York, 1992.

(21) Kramer, L. *J. Chem. Phys.* **1971**, *55*, 2097.

(22) Bouchiat, A. M.; Langevin, D. *J. Colloid Interface Sci.* **1978**, *63*, 193.

(23) Kawaguchi, M. *Prog. Polym. Sci.* **1993**, *18*, 341.

(24) Earnshaw, J. C. *Adv. Colloid Interface Sci.* **1996**, *68*, 1.

was Millipore grade-Q deionized and double distilled, with a resistivity higher than 18 M Ω cm.

Synthesis of Bis(*p*-(2-hydroxy)ethoxyphenyl)diazomethane (4). A solution of 0.23 mmol (70 mg) of **3** (obtained from 4,4'-dihydroxybenzophenone (**2**) with 2-bromoethanol (**1a**) in the presence of KOH in EtOH/H₂O and catalytic amounts of IK), hydrazine monohydrate (8.54 mmol, 428 mg), and hydrazine dihydrochloride (1.26 mmol, 132 mg) in ethanol (20 mL) was refluxed for 24 h.²⁵ The solution was diluted with Et₂O and poured into water, the aqueous phase was separated and extracted with Et₂O, and the combined organic layers were washed with water, dried (Na₂SO₄), and evaporated. The residue was dried in vacuo to afford the hydrazone (70 mg, 96%). ¹H NMR (DMSO-*d*₆): δ 7.25 (d, 2H, *J* = 8.9 Hz, H-Ar), 7.23 (s, 4H, H-Ar), 6.85 (d, 2H, *J* = 8.9 Hz, H-Ar), 6.01 (sa, 2H, NH₂), 4.90 (q, 2H, CH₂O), 4.05 (t, 2H, *J* = 4.9 Hz, CH₂O), 3.96 (t, 2H, *J* = 4.9 Hz, CH₂O), 3.73 (qa, 4H, CH₂O, 2 OH) ppm. IR (KBr): ν 1608, 1508, 1450, 1247, 1168, 1082, 1049, 904, 829 cm⁻¹.

To a solution of hydrazone (0.24 mmol, 76 mg) in THF (20 mL) was added Na₂SO₄ (48 mg), HgO (0.36 mmol, 78 mg), and catalytic amounts of KOH in EtOH.²⁶ The mixture was stirred at 70 °C, under argon and protected from light, for 5 h. Violet solid was filtered and washed with THF. A 72.5 mg (96%) quantity of bis(*p*-(2-hydroxy)ethoxyphenyl)diazomethane (**4**) was obtained. ¹H NMR (CDCl₃): δ 7.19 (d, 4H, *J* = 5.8 Hz, H-Ar), 6.97 (d, 4H, *J* = 5.8 Hz, H-Ar), 4.13–4.09 (m, 4H, OCH₂), 4.04–3.99 (m, 6H, CH₂OH, 2OH) ppm. ¹³C NMR (DMSO-*d*₆): δ 157.0 (2C, C-4, Ar), 126.2 (4C, Ar), 120.1 (2C, C-1, Ar), 115.6 (4C, Ar), 79.1 (CN₂), 69.6 (2C, CH₂O), 59.5 (2C, CH₂O) ppm. IR (KBr): ν 2029, 1635, 1558, 1508, 1458, 1249, 1091, 1053, 831 cm⁻¹.

Synthesis of Spiro[1'-(bis(*p*-(2-hydroxy)ethoxyphenyl))-1',61-methano-60-fullerene (5). A solution of C₆₀ (0.30 mmol, 216 mg) and the diazomethane **4** (0.30 mmol, 94 mg) in ODCB (30 mL) was stirred at reflux for 24 h. The solvent was then evaporated, and the crude material was chromatographed on a silica gel column (toluene/methanol, 15:1) after which 105 mg (35%) of fullerene derivative **5** was obtained. Mp > 300 °C. ¹H NMR (CDCl₃, 300 MHz): δ 8.01 (d, 4H, *J* = 5.6 Hz, H-Ar), 7.03 (d, 4H, *J* = 5.6 Hz, H-Ar), 4.13 (m, 4H, OCH₂), 3.98 (m, 4H, CH₂OH). ¹³C NMR (CDCl₃/CS₂, 75 MHz): δ 158.7, 148.6, 145.7, 145.6, 145.2, 145.2, 144.8, 144.3, 143.4, 142.6, 142.5, 141.6, 138.7, 132.4, 132.2, 115.2, 79.7, 69.9, 62.0, 30.6. IR (KBr): ν 1608, 1508, 1245, 1174, 1078, 1041, 821, 557, 526 cm⁻¹. UV-vis λ (DMSO/H₂O): 258, 328, 430, 698 nm. MS M⁺ (FAB⁺) 1006.9.

Synthesis of *p*-(6-Hydroxy)hexanoxybenzaldehyde (7). 4-Hydroxybenzaldehyde (1.64 mmol, 200 mg), 6-brom-1-hexanol (1.64 mmol, 300 mg), and K₂CO₃ (1.64 mmol, 64.12 mg) were refluxed in acetone (5 mL) for 16 h. Solids were filtered and washed with acetone, and the volatiles were removed in vacuo. The resulting product was further purified by column chromatography (hexane/EtOAc, 2:1) to yield 150 mg (41%) of the *p*-benzaldehyde derivative **7**. ¹H NMR (CDCl₃): δ 9.85 (s, 1H, CHO), 7.81 (d, 2H, *J* = 5.8 Hz, H-Ar), 6.97 (d, 2H, *J* = 5.8 Hz, H-Ar), 4.03 (t, 2H, *J* = 4.2 Hz, OCH₂), 3.65 (t, 2H, *J* = 4.2 Hz, CH₂OH), 1.81 (m, 2H), 1.59 (m, 2H), 1.48–1.42 (m, 5H) ppm.

Synthesis of *N*-Methyl-2-[*p*-(6-hydroxy)hexanoxyphenyl]pyrrolidine[3,4:1,2][60]fullerene (9). A toluene solution containing C₆₀ (0.277 mmol, 200 mg), *N*-methylglycine (1.38 mmol, 123.3 mg), and the aldehyde **7** (0.277 mmol, 61.5 mg) was heated to reflux for 10 h.²⁷ The solvent was then evaporated and the crude material chromatographed on a silica gel column (toluene/EtOAc, 4:1) after which 94 mg (35%) of fullerene derivative **9** was obtained. Mp > 300 °C. ¹H NMR (CDCl₃): δ 7.69 (ba, 2H, H-Ar), 6.94 (d, 2H, *J* = 5.7 Hz, H-Ar), 4.97 (d, 1H, *J* = 6.3 Hz, CH₂N), 4.87 (s, 1H, CHN), 4.24 (d, 1H, *J* = 6.3 Hz, CH₂N), 3.96 (t, 2H, *J* = 4.3 Hz, CH₂OH), 3.65 (t, 2H, *J* = 4.3 Hz, CH₂O), 2.79 (s, 3H, CH₃N), 1.81–1.75 (m, 2H), 1.58–1.42 (m, 6H). ¹³C NMR (CDCl₃/CS₂, 75 MHz): δ 159.1, 147.1, 146.3, 146.2, 146.1, 146.0, 145.8, 145.5, 145.4, 145.3, 145.2, 145.1, 144.6, 144.2, 143.0, 142.9, 142.6, 142.5, 142.4, 142.1, 142.0, 141.9, 141.8, 141.7,

141.5, 141.4, 140.0, 139.8, 135.6, 130.3, 114.5, 83.1, 77.2, 68.7, 67.6, 62.8, 39.8, 32.7, 29.3, 25.9, 25.6. IR (KBr): ν 2929, 2907, 2857, 2776, 1608, 1510, 1461, 1426, 1245, 1170, 526 cm⁻¹. UV-vis λ _{max} (toluene): 288, 310, 434 nm. MS M⁺ (FAB⁺) 969.9.

Protection of 11-Brom-1-undecanol. 11-Brom-1-undecanol (**1c**) (3 mmol, 753.6 mg) was dissolved in dimethoxymethane (4 mL), and 0.6 mmol of BrLi and 0.27 mmol of *p*-toluenesulfonic acid were added. The reaction mixture was stirred at room temperature for 24 h. H₂O was added to the reaction, and the mixture was extracted with Et₂O, washed with saturated solution of NaCl, and dried over MgSO₄, and the volatiles were removed in vacuo. The resulting residue was purified by flash chromatography (hexane/EtOAc, 8:1) to yield 720 mg of protected product (81.5%). ¹H NMR (CDCl₃): δ 4.55 (s, 2H, BrCH₂), 3.45 (t, 2H, *J* = 6.6 Hz, CH₂O), 3.34 (t, 2H, *J* = 6.6 Hz, OCH₂O), 3.29 (s, 3H, OCH₃), 1.81–1.71 (m, 2H), 1.57–1.48 (m, 2H), 1.21 (m, 14H) ppm.

Synthesis of *p*-(11-Hydroxy)undecanoxybenzaldehyde (8). 4-Hydroxybenzaldehyde (122.12 mg, 1 mmol), the protected 11-brom-1-undecanol (2 mmol, 589.8 mg), and K₂CO₃ (2.9 mmol, 400 mg) were refluxed in acetone (5 mL) for 16 h. The solids formed were filtered and washed with acetone, and the volatiles were removed in vacuo. The product obtained was purified by column chromatography (hexane/EtOAc, 2:1) to yield 300 mg (89%) of protected benzaldehyde derivative. ¹H NMR (CDCl₃): δ 9.81 (s, 1H, CHO), 7.75 (d, 2H, *J* = 8.7 Hz, H-Ar), 6.92 (d, 2H, *J* = 8.7 Hz, H-Ar), 3.96 (t, 2H, *J* = 6.5 Hz, OCH₂), 3.44 (t, 2H, *J* = 6.5 Hz, OCH₂), 3.33 (t, 2H, *J* = 6.9 Hz, OCH₂O), 3.29 (s, 3H, OCH₃), 1.84–1.67 (m, 2H), 1.55–1.45 (m, 2H), 1.23 (m, 14H) ppm. ¹³C NMR (CDCl₃): δ 190.6 (CHO), 164.11 (C-4, Ar), 131.8 (2C, C-2, C-6, Ar), 129.6 (C-1, Ar), 114.6 (2C, C-3, C-5, Ar), 96.2 (OCH₂O), 68.3 (Ar-OCH₂), 67.7 (CH₂O), 59.9 (CH₃O), 33.8, 32.7, 29.2, 29.1, 28.9, 28.6, 28.0, 26.0, 25.8 ppm.

This compound was hydrolyzed, quantitatively, by dilute hydrochloric acid in methanol to give **8**. ¹H NMR (CDCl₃): δ 9.81 (s, 1H, CHO), 7.75 (d, 2H, *J* = 8.7 Hz, H-Ar), 6.92 (d, 2H, *J* = 8.7 Hz, H-Ar), 3.96 (t, 2H, *J* = 6.5 Hz, CH₂OH), 3.57 (t, 2H, *J* = 6.5 Hz, OCH₂), 1.80–1.67 (m, 2H), 1.49–1.23 (m, 17H) ppm. ¹³C NMR (CDCl₃): δ 190.8 (CHO), 164.2 (C-4, Ar), 131.9 (2C, C-2, C-6, Ar), 129.7 (C-1, Ar), 114.7 (2C, C-3, C-5, Ar), 68.4 (OCH₂), 63.0 (CH₂OH), 32.7, 29.5 (2C), 29.4, 29.3, 29.2, 29.0, 25.9, 25.7 ppm.

Synthesis of *N*-Methyl-2-[*p*-(11-hydroxy)undecanoxyphenyl]pyrrolidine[3,4:1,2][60]fullerene (10). A toluene solution containing C₆₀ (0.277 mmol, 200 mg), *N*-methylglycine (1.38 mmol, 123.3 mg), and the aldehyde **8** (0.277 mmol, 80.8 mg) was heated to reflux for 10 h. The solvent was then evaporated, and the crude material chromatographed on a silica gel column (toluene/EtOAc, 4:1) after which 90 mg (31%) of fullerene derivative was obtained. Mp > 300 °C. ¹H NMR (CDCl₃/CS₂, 300 MHz): δ 7.67 (s, br, 2H, H-Ar), 6.91 (d, 2H, *J* = 8.6 Hz, H-Ar), 4.97 (d, 1H, *J* = 9.3 Hz, CH₂N), 4.88 (s, 1H, CHN), 4.25 (d, 1H, *J* = 9.3 Hz, CH₂N), 3.94 (t, 2H, *J* = 6.5 Hz, CH₂OH), 3.63 (t, 2H, *J* = 6.5 Hz, CH₂O), 2.80 (s, 3H, CH₃N), 1.78 (m, 2H), 1.56–1.27 (m, 17H). ¹³C NMR (CDCl₃/CS₂, 75 MHz): δ 159.0, 156.1, 153.8, 153.4, 153.3, 147.0, 146.6, 146.3, 146.2, 146.1, 146.04, 146.00, 145.95, 145.91, 145.90, 145.7, 145.6, 145.4, 145.3, 145.28, 145.24, 145.15, 145.1, 145.04, 145.00, 144.9, 144.5, 144.4, 142.9, 142.8, 142.5, 142.4, 142.4, 142.3, 142.1, 142.0, 141.95, 141.92, 141.90, 141.83, 141.8, 141.7, 141.6, 141.5, 141.3, 140.0, 139.9, 139.7, 139.4, 136.6, 136.4, 135.6, 130.2, 128.3, 114.4, 83.0, 77.1, 69.8, 68.7, 67.7, 62.9, 39.8, 32.9, 29.7, 29.64, 29.62, 29.5, 29.4, 26.2, 25.8. IR (KBr): ν 2922, 2850, 2775, 1608, 1509, 1461, 1425, 1243, 1169, 525 cm⁻¹. UV-vis λ _{max} (toluene): 302, 434 nm. MS M⁺ (FAB⁺) 1040.0.

2.b. Synthesis of C60 Derivatives. The synthesis of methanofullerene (**5**) has been carried out in three steps from commercially available 2-bromoethanol (**1a**) and 4,4'-dihydroxybenzophenone (**2**) as is depicted in the Scheme 1. Thus, esterification reaction from **1a** and **2** leads to compound **3** bearing two hydroxylic groups.

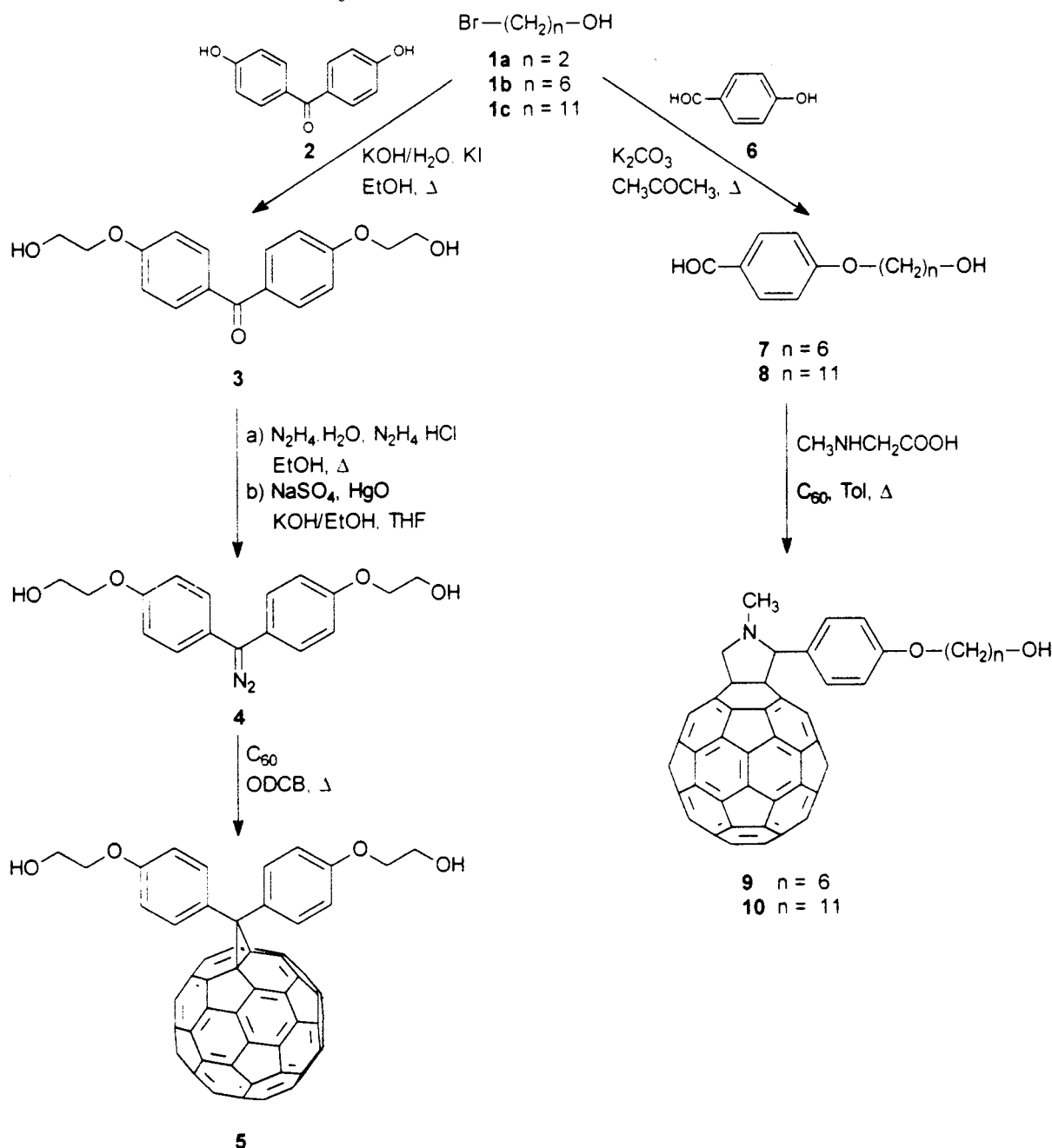
Dihydroxyethoxybenzophenone (**3**) was transformed into the corresponding diazocompound (**4**) by treatment with hydrazine hydrate and further oxidation reaction. Diazocompounds have been previously reported to react with C₆₀ to form the fulleroid as the kinetic product and/or the thermodynamically more stable

(25) Tomioka, H.; Yamamoto, K. *J. Chem. Soc., Perkin Trans. 1* **1996**, 63.

(26) Bak, C.; Praefcke, K. *Chem. Ber.* **1979**, *112*, 2744.

(27) Maggini, M.; Scorrano, G.; Prato, M. *J. Am. Chem. Soc.* **1993**, *115*, 9798. For a recent review, see: Prato, M.; Maggini, M. *Acc. Chem. Res.* **1998**, *31*, 519.

Scheme 1. Synthesis of Functionalized Derivatives 5, 9, and 10



methanofullerene.²⁸ In our case, methanofullerene (**5**) was obtained as the only product in 35% yield.

Fulleropyrrolidines **9** and **10** were prepared by 1,3-dipolar cycloaddition reaction of the in situ formed azomethine ylide, from sarcosine (*N*-methylglycine) and the respective aldehyde (**7**, **8**), to C_{60} by following Prato's procedure. Hydroxyfunctionalized benzaldehydes endowed with long alkyl chains (**7**, $n = 6$; **8**, $n = 11$) were in turn prepared by esterification reaction of *p*-hydroxybenzaldehyde (**6**) with the respective bromoalkanol (**1**). It is worth mentioning that formation of compound **8** from hydroxyl-protected derivative of **1c** leads to remarkably higher yields in comparison with the reaction using unprotected alcohol (**1b**).

The structure of the novel compounds prepared was ascertained by using analytical and spectroscopic procedures. All the fullerene derivatives showed the band at around 430 nm in their electronic spectra typical of 1,2-dihydrofullerenes. The ^1H NMR spectra of fulleropyrrolidines (**9**, **10**) exhibit the pyrrolidine

protons as two doublets at δ 4.9 and 4.2 ppm (CH_2 group) and the CH at δ 4.8 ppm. Methanofullerene **5** presents, in addition of the aromatic protons, the methylene groups at δ 4.13 and 3.98 ppm as multiplets.

2.c. Monolayer Measurements. Spread monolayers were formed by adding small amounts of benzene solutions of the studied compounds with a microsyringe (Hamilton) in a commercial Teflon trough (KSV Minitrough). These organic solutions were filtered through a $0.2 \mu\text{m}$ Teflon membrane (Millipore) before use. The solutions were just prepared before use to avoid aggregation phenomena similar to those described by Ying et al.²⁹ The Π - A compression isotherms were recorded at 298 K by the continuous method, after spreading a small quantity ($\sim 50 \mu\text{L}$) of a highly diluted solution. The initial state of the film was always chosen to have a surface pressure, Π , close to zero. After total evaporation of the solvent and stabilization of the film (typically ~ 10 min), the film is continuously and symmetrically compressed by the action of two opposite barriers (Delrin). The compression speed was then maintained constant about 1 \AA^2

(28) Suzuki, T.; Li, Q.; Khemani, K. C.; Wudl, F. *J. Am. Chem. Soc.* **1992**, *114*, 7301. Schick, G.; Hirsch, A. *Tetrahedron* **1998**, *54*, 4283.

(29) Ying, Q.; Marecek, J.; Chu, B. *Chem. Phys. Lett.* **1994**, *219*, 214.

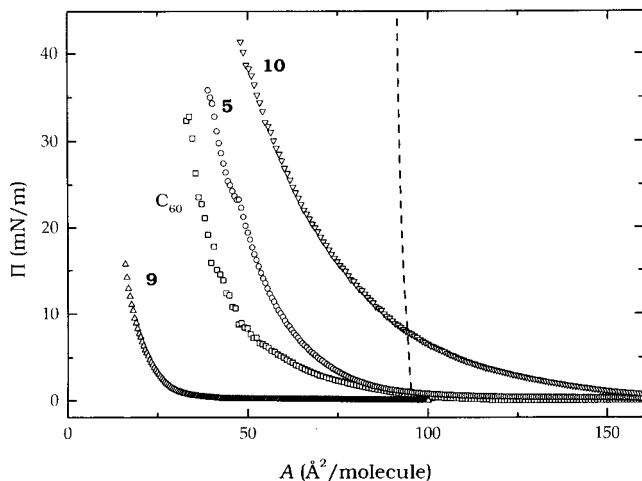


Figure 2. Surface pressure–molecular area (Π – A) isotherms at 298 K of the pure films of C_{60} and the derivatives **5**, **9**, and **10** on a 10^{-2} M HCl aqueous subphase. The dashed line reproduces the isotherm reported by Öbeng and Bard (ref 7) for a monolayer of pure C_{60} .

Table 1. Limit Areas for the Monolayers of the Different Fullerene Derivatives

fullerene	A_0 ($\text{\AA}^2/\text{molecule}$)	
	full Π range	only $\Pi < 20$ mN/m
pure C_{60}	46 ± 5	57 ± 10
5	60 ± 6	66 ± 3
9	25 ± 3	25 ± 3
10	84 ± 2	107 ± 5

molecule $^{-1}$ min $^{-1}$. Surface pressure was measured by a Pt–Wilhelmy balance with accuracy ± 0.05 mN/m. The evaporation losses in the subphase were prevented by enclosing the trough in a Plexiglas box, which was maintained under a continuous nitrogen flow saturated with water.

2.d. Surface Quasi-Elastic Light Scattering (SQELS). The surface light scattering apparatus has been described elsewhere.^{20,30} Briefly, a polarized intensity stabilized laser beam (He–Ne 25 mW) was spatially filtered to ensure a clean expanded Gaussian intensity profile. The beam passes through a diffraction grating and then a focusing lens, forming a 1:1 image of the spot on the grating on top of the liquid surface. The light scattered by thermally excited capillary waves is mixed in the detector with each diffraction order reflected by the surface (heterodyne detection). This allows one the selection of the wavevector, q . The output of the detector, a photomultiplier (Hamamatsu R1104), goes to an amplifier/band-pass filter (SR 560), which accommodates the signal entry in a FFT spectrum analyzer (SR 760). The observed spectrum is a convolution between the theoretical spectrum and an instrumental broadening contribution, which produces a smearing out of the details of the spectra. As a consequence, minimization of the instrumental contribution is crucial.

3. Results and Discussion

3.a. Equilibrium Properties. 3.a.1. Langmuir Films of the Pure Compounds. Figure 2 shows the compression isotherms obtained at 298 K corresponding to the spread films of pure C_{60} and derivatives **5**, **9**, and **10** on the free surface of the subphase (pH = 2). To better rationalize these results, Table 1 collects the limiting area of these isotherms calculated by extrapolating at $\Pi = 0$, corresponding to the linear part of the high-pressure branch. The Π – A curves for pure C_{60} and derivative **5** start to increase at $A \sim 100$ \AA^2 , a value similar to the limiting area reported by Öbeng and Bard⁷ for a film of

pure C_{60} following a similar protocol. However, our experimental isotherm for C_{60} is more compressed (Π starts to grow at lower molecular areas). It shows also a smoother Π increase than that of ref 7, and it is more similar to the results described by other authors.^{10,14} We can conclude that the data correspond to a multilayer arrangement.

The Π – A isotherm for compound **5** is more expanded than that of pure C_{60} but shows the same qualitative features. The limiting area for this bichained derivative is obtained to be significantly larger than the value obtained for pure C_{60} , $A_0 = 60 \pm 6$ \AA^2 . This seems to indicate a weak grafting effect of the two phenoxyethanol functions at the air–water interface, in agreement with the results reported by Ravaine et al.¹⁴ for a similar fullerene derivative. These authors indicate that due to the rigidity of the fullerene films in the high pressure states ($\Pi > 20$ mN/m), the Wilhelmy plate is pushed out from the surface, leading to low apparent Π values. If this part of the experimental isotherm is not taken into account, we obtain then limiting areas of 57 ± 10 and 66 ± 3 \AA^2 (see Table 1) for pure C_{60} and the bichained derivative (**5**), respectively, in agreement with the results from Ravaine et al.¹⁴ A small kink at $\Pi \sim 23.3$ mN/m and $A \sim 47.5$ \AA^2 is also observed in the isotherm of derivative **5**, probably corresponding to formation of a bilayer (it occurs at an area half that of the cross section of a C_{60} sphere, ~ 90 \AA^2).

Figure 2 shows that the fullerene derivative **9**, with only one amphiphilic function, leads to a very compressed isotherm, $A_0 = 25 \pm 3$ \AA^2 . This suggests a strong aggregation at the air–water interface. This agrees with the results previously reported for other fullerene derivatives with similarly slightly polar functional groups.¹⁴ Although the phenoxyhexanol amphiphilic rest might have some surfactant character, the hydrophobic–hydrophilic balance is small due to the small chain length. As a consequence, from the energetic point of view, fullerene aggregation may be more favorable than adsorption onto the surface. The adsorption energy, $\Pi A \sim 2 \times 10^{-21}$ J molecule $^{-1}$ at 298 K and at the highest surface pressure observed for this derivative ($\Pi \sim 13$ mN/m), is lower than the thermal energy $k_B T$ and therefore the aggregated state is the more stable phase for this compound. However, as seen in Figure 2, its homologous with 11 carbons (compound **10**) is able to form monolayers. This isotherm is characterized by a limiting area, $A_0 = 84 \pm 2$ \AA^2 , a value close to the cross-sectional area of a single fullerene molecule. The adsorption energy per molecule at this area is $\Pi A \sim 3 k_B T$, thus anchoring at the air–water is favored with respect to tridimensional aggregation. The important difference between the interfacial behavior of compounds **9** and **10** may be thus attributed to the balance between the adsorption forces (proportional to the chain length) and the net hydrophobicity (mainly governed by the fullerene core).

Concerning derivative **10**, the only one able to form a stable monolayer at the air–water interface, no transition plateaus are observed in the Π – A curve within the experimental accuracy. This means that if a solidlike phase exists at small areas, $A \leq \sigma \sim 87$ \AA^2 , it appears continuously from a disordered low-pressure fluid phase; however more experimental work is needed in order to clarify this point. The equilibrium elastic properties of this monolayer can be characterized from the static compression modulus ϵ_0 , defined for an insoluble monolayer, $A \equiv 1/\Gamma$, as follows:

$$\epsilon_0 = \Gamma \left(\frac{\partial \Pi}{\partial \Gamma} \right)_T = -A \left(\frac{\partial \Pi}{\partial A} \right)_T \quad (2)$$

Figure 3 shows that this parameter increases monoto-

(30) Monroy, F.; Ortega, F.; Rubio, R. G. *Phys. Rev. E* **1998**, *58*, 7629.

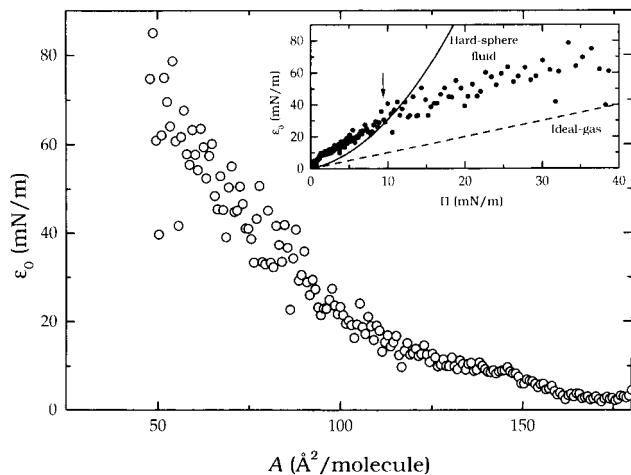


Figure 3. Equilibrium elasticity modulus ϵ_0 for the monolayer of derivative **10** spread on a 10^{-2} M HCl aqueous subphase at 298 K. The inset compares the Π dependence of the experimental values of ϵ_0 with the theoretical prediction for a noninteracting 2D gas and a hard-sphere fluid.

nously when the monolayer of **10** is compressed; as it can be observed in the inset of the figure, the compression modulus always exceeds the value of surface pressure ($\epsilon_0/\Pi > 1$). This may be due to the high degree of packing of the fullerene molecules in the concentration range studied here. Even at the largest areas studied, $A \sim 160 \text{ \AA}^2$, the packing degree is $1/2$, i.e., in this state the center-to-center distance is in average $\sqrt{2}D_{C_{60}} \sim 15 \text{ \AA}$, a value close to the diameter of a single fullerene molecule, $D_{C_{60}} \sim 10.6 \text{ \AA}$, corresponding to the closest-packing distance. These excluded-volume repulsive effects are clearly pointed out in the inset of Figure 3. It compares the experimental ϵ_0 - Π data with the theoretical prediction for isothermal compressibility from a bidimensional ideal gas equation of state, $\Pi A = k_B T$, and for the hard-sphere bidimensional fluid, $\Pi(A - A_{\text{excl}}) = k_B T$, with $A_{\text{excl}} = \sigma = 87 \text{ \AA}^2$. The observed elasticities are always larger than those expected for a noninteracting gas; at the lowest surface pressures, they are even slightly larger than the values predicted from the excluded-area correction. This low-pressure behavior ($\Pi < 10 \text{ mN/m}$ and $A \geq 90 \text{ \AA}^2 > \sigma$) points out that a fullerene sphere, with a 11C grafted alkyl chain, excludes more area than the geometrical size of a simple fullerene molecule. When this bidimensional system is compressed further, $A < \sigma = 87 \text{ \AA}^2$, the fullerene spheres come into mutual contact; if they would behave like hard impenetrable objects, then $\epsilon_0 = \Pi/(1 - A_{\text{excl}}/A)$, diverging at $A < A_{\text{excl}}$ (zero compressibility). The experimental behavior is found to be intermediate between the noninteracting ($\epsilon_0 = \Pi$) and the pure-repulsive volume excluded cases, suggesting the existence of very-short-range attractive forces, responsible, for instance, for the observed finite elastic behavior and cohesion in the monolayer.

3.a.2. Mixed Films. PDA + C_{60} . Although the monolayers of fatty acids have been extensively studied in the literature, for the sake of clarity and homogeneity in the discussion of the results of the blends PDA + fullerenes, Figure 4 reproduces here the isotherm obtained for pure PDA. Briefly, the gas (G) phase of the PDA monolayer exists only at low pressure ($\Pi < 0.5 \text{ mN/m}$) and large molecular areas, $A_G > 50 \text{ \AA}^2 \text{ molecule}^{-1}$, while the liquid expanded (LE) phase appears in compressing at smaller areas. This disordered LE phase is present only at molecular areas larger than $A_{LE} \sim 29 \text{ \AA}^2 \text{ molecule}^{-1}$ and $\Pi < 8 \text{ mN/m}$ (values in agreement with those reported by

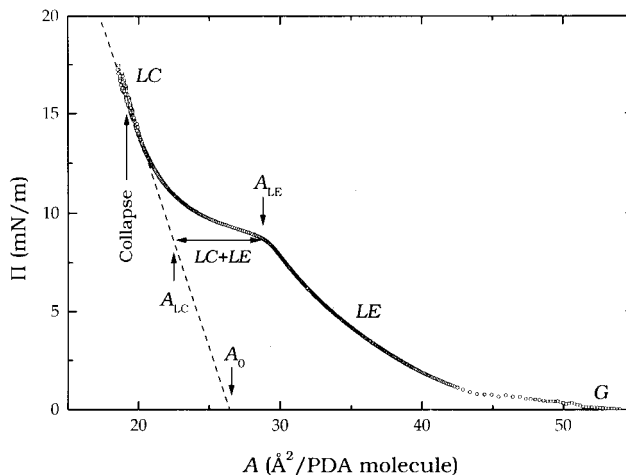


Figure 4. Π - A experimental isotherm at 298 K of the monolayer of pure pentadecanoic acid (PDA) spread on an aqueous subphase acidified at pH = 2 (symbols are defined in the text).

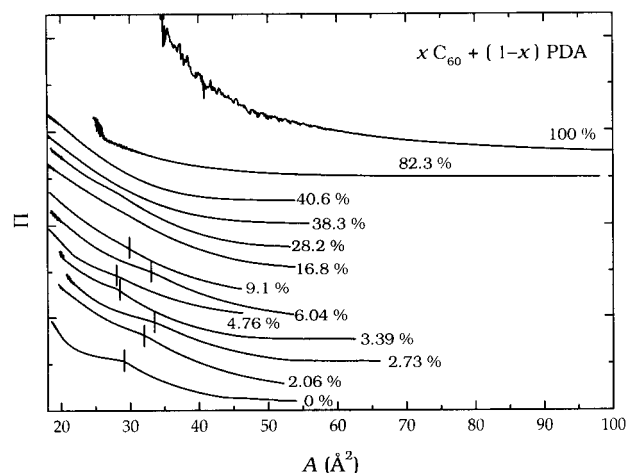


Figure 5. Π - A experimental isotherms of the mixed films of pure C_{60} with PDA spread on an aqueous subphase acidified at pH = 2 and at 298 K. The figures near each isotherm refer to the C_{60} -molar fraction of the blend. For the sake of clarity, each isotherm has been shifted 5 mN m^{-1} upward with respect to the previous one.

Harkins and Boyd at the same temperature).³¹ At this point a smooth coexistence plateau with a more ordered liquid condensed (LC) phase appears. At molecular areas smaller than $A_{LC} \sim 21 \text{ \AA}^2 \text{ molecule}^{-1}$, only the LC phase is present. This phase is an ordered fluid with short-range order and lacking long-range crystalline order.

It is customary to characterize the LC phase from the values of the limiting area per molecule, A_0 .³² From the isotherm in Figure 4 we obtain $A_0 = 26.4 \pm 0.8 \text{ \AA}^2$ for a PDA molecule at the air-water interface, in agreement with the values reported in the literature.³¹ Figure 4 shows how to make a rough estimation of the LC boundary of the LE/LC coexistence plateau: First one makes a linear extrapolation of the LC branch (it should be linear if free of kinetics effects arising from the compression method³²). Then, one calculates its intercept with the $\Pi_{LE} = \Pi(A = A_{LE}) = \text{constant}$ coexistence branch of the isotherm in the ideal equilibrium state. We then calculate $A_{LC} \sim 22.5 \text{ \AA}^2$ for the

(31) Harkins, W. D.; Boyd, E. *J. Phys. Chem.* **1945**, *42*, 20.

(32) Gaines G. L. *Insoluble Monolayers at Liquid-Gas Interfaces*; Wiley: New York, 1966.

(33) Moore, B. G.; Knobler, C. M.; Akamatsu, S.; Rondelez, F. *J. Phys. Chem.* **1990**, *94*, 4588.

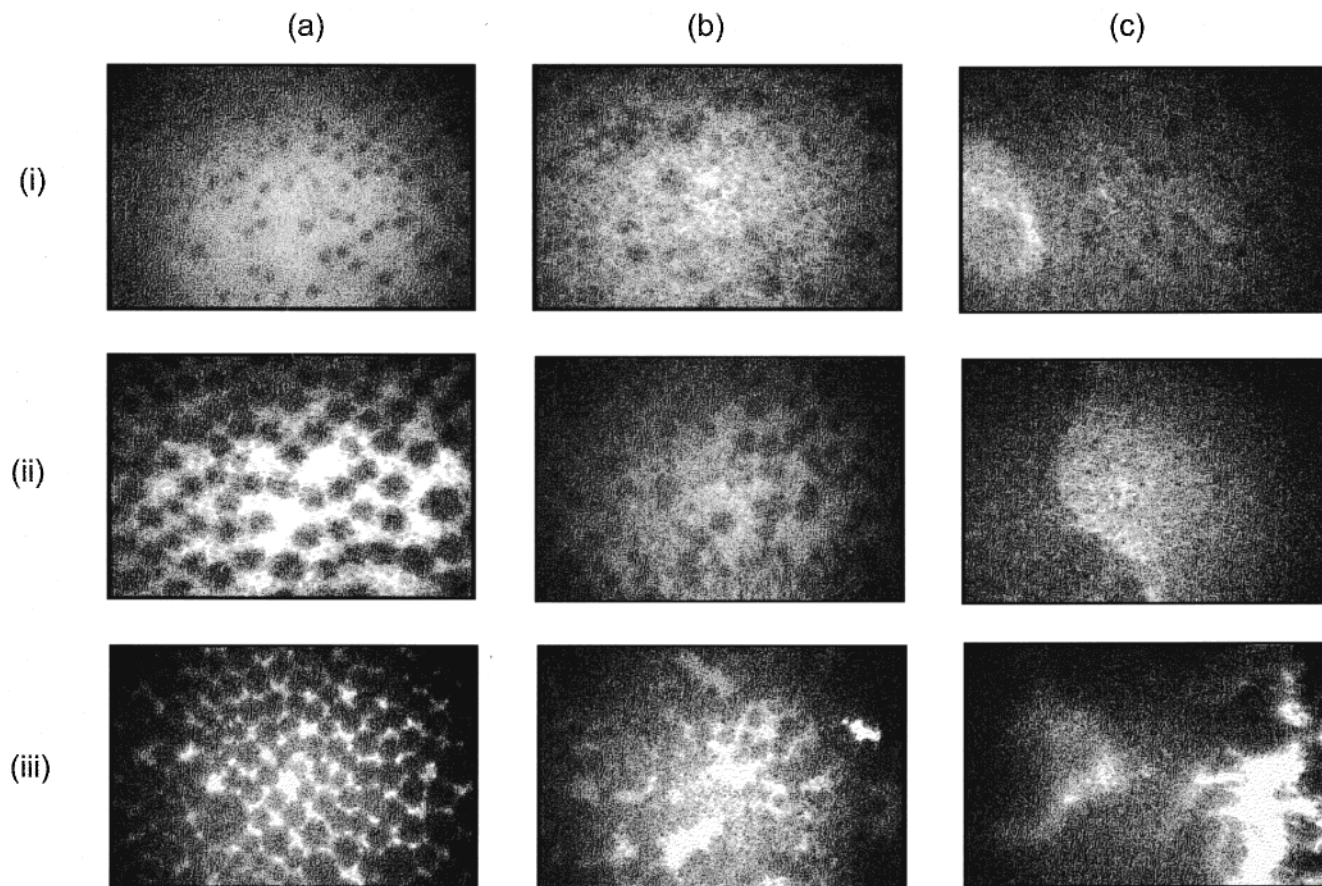


Figure 6. Fluorescence microscopy photographs of mixed films of C_{60} + PDA at the air–water interface (see text for explanation). 1 mol % of NBD-hexadecylamine has been used as fluorescent probe. The width of each image corresponds to 200 μm .

PDA monolayer at 298 K, in agreement with the value reported by Moore et al.³³

Figure 5 shows some of the experimental isotherms for the films of the $x C_{60} + (1 - x) \text{PDA}$ blend, x being the C_{60} molar fraction. The molecular area of the mixtures, A , is calculated from the total molar concentration in the insoluble film, i.e., $A = \Gamma^{-1} = (\Gamma_{C_{60}} + \Gamma_{\text{PDA}})^{-1}$. For the sake of clarity, the Π axis has been successively rescaled by a fixed increment of $\Delta\Pi = +5$ mN/m for each Π – A curve. It can be easily observed that the transitional LE–LC plateau characteristic of the isotherm of pure PDA appears progressively blurred as the monolayers becomes richer in C_{60} ; no discernible plateau is observed at compositions larger than 16% in C_{60} (mole fraction of C_{60} , $x \geq 0.1$).

To understand this phase transition, we have studied the morphology of the monolayers of three different blends (pure PDA and 5% and 15% in C_{60}) by using epifluorescence microscopy.³⁴ Figure 6 shows the textures observed in these monolayers in three different surface states around the LE–LC transition: (i) at the beginning of the transition, $A \sim A_{\text{LE}}$; (ii) at the middle of this transitional region; (iii) and in the low area boundary, $A \sim A_{\text{LC}}$. The pure PDA monolayer (Figure 6a) exhibits the characteristic uniform distribution of dark domains of LC phase (which exclude the fluorescent probe), which become closer with increasing surface concentration. This distribution appears to be a bit more disordered for the 5% blend (Figure 6b). Apparently, there are no tridimensional patches of C_{60} aggregates, which should preferentially absorb the fluorescent probe, because of its high hydrophobicity and more disordered character than that of the 2D arrange-

ments. If C_{60} was segregated from the ordered LC phase, an accumulation of these molecules in the background of the PDA–LE phase should take place, becoming then locally brighter if the fluorescent probes, within C_{60} , aggregate. This is however the case of the richer- C_{60} blend at 15% (Figure 6c). No LC domains are now clearly observed, coinciding with the disappearance of the transitional plateau in the Π – A isotherm. In addition, aggregated 3D structures are now clearly visible all the way from the starting point at a low- Π state, to the monolayer's collapse (Figure 6c,i–iii). The morphology then becomes inhomogeneous, characteristic of a multi-layer arrangement in equilibrium with the monolayer.

In the PDA-rich composition range ($x < 0.15$), the whole isotherm shifts to larger areas with increasing x , reaching a maximum expansion at a composition close to 15% in C_{60} molecules (see Figure 7). This composition coincides with that of a compatible mixed condensed monolayer with hexagonal unit cells, and in which there is a C_{60} molecule per unit cell surrounded by six PDA molecules ($x = 14\%$). Hence the following picture might be suggested: for low values of $x (< 0.15)$ the hexagonal structure of the PDA monolayer in the LC phase is possible, and the PDA molecules can accommodate all the C_{60} molecules within an ordered hexagonal structure. For $x > 0.15$, the PDA matrix monolayer is no longer able to stabilize the system, and C_{60} aggregation takes place.

(35) Goodrich, F. C. *Proceedings of the 2nd International Congress on Surface Activity*; Butterworth: London, 1957.

(36) Joos, P.; Demel, R. A. *Biochim. Biophys. Acta* **1969**, *183*, 447.

(37) Sun Y.-P., In *Molecular and Supramolecular Photochemistry*; Ramamurthy, V., Schanze, K., Eds.; Marcel Dekker: New York, 1997; Vol. 1, 325.

(34) Knobler, C. M. *Adv. Chem. Phys.* **1990**, *77*, 397.

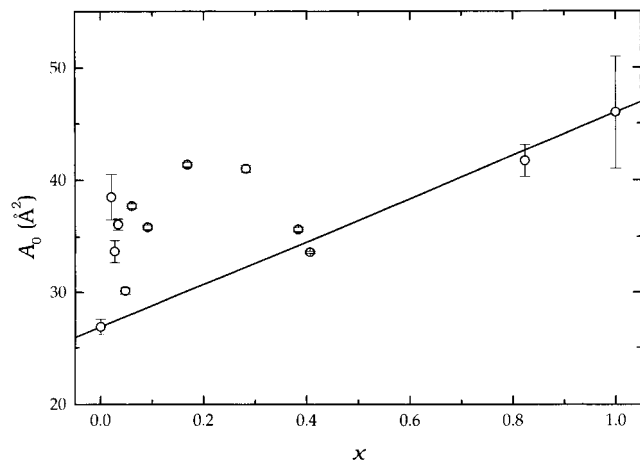


Figure 7. Limiting areas of the isotherms of spread films of the $x\text{C}_{60} + (1-x)\text{PDA}$ blend. The continuous line accounts for the ideal-like behavior of the mixing limiting areas, i.e., $A_0^{\text{ideal}} = xA_{\text{C}_{60}} + (1-x)A_{\text{PDA}}$.

For a miscible binary film, it is well-known that the collapse pressure must vary with composition between the values for the pure-component monolayers^{35,36}

$$x_1 a_1 \exp\left[\frac{\Pi^{(c)} - \Pi_1^{(c)}}{k_B T} A_1^{(c)}\right] + x_2 a_2 \exp\left[\frac{\Pi^{(c)} - \Pi_2^{(c)}}{k_B T} A_2^{(c)}\right] \equiv 1 \quad (3)$$

where $\Pi^{(c)}$ and $A_i^{(c)}$ represent surface pressure and molecular area at collapse, respectively, and a_i is the activity coefficient of the i constituent in the film. On the other hand, if both components are incompatible in the film, at collapse, the less stable component is segregated. Two different phases are then present and $\Pi^{(c)}$ becomes independent of composition and equal to the smaller pure-component value. One can see that this is the case of mixed films of PDA + C_{60} at $x > 0.2$ from the collapse pressures obtained from the isotherms in Figure 5; $\Pi^{(c)}$ remains approximately constant in a value near to 20 mN/m, the value corresponding to a pure PDA monolayer. A slight x dependence of the collapse pressure is observed at $x < 0.2$, supporting the idea of film compatibility for the diluted- C_{60} blends. However, such a Π variation is not detected for the pressure at which the LE/LC transitions begin, which remains almost constant in ca. 10 mN/m.

To check for such incompatible-like general behavior of the PDA + C_{60} blend, we have carried out a thermodynamic analysis of the excess quantities. As a first approach, we calculate the excess areas, $A_E = A - A^I = A - [xA_{\text{C}_{60}} + (1-x)A_{\text{PDA}}]$, which are close to zero in the PDA-richer side ($x < 0.2$) and become strongly negative, $A^E \sim -15 \text{ \AA}^2$, at compositions richer in fullerene. Values of $A^E < 0$ may be rationalized in terms of two different antagonist factors: cohesive interactions between PDA and C_{60} molecules favoring film stability and miscibility, and excluded volume interactions from PDA, which could promote and/or reinforce segregation and further aggregation of C_{60} . As a consequence, in both cases, miscible or immiscible respectively, denser states ($A^E < 0$) will be observed for the mixtures. From the excess areas it is possible to calculate the excess free energy ΔG^E as follows³²

$$\Delta G^E(\Pi) = \int_0^\Pi A^E d\Pi \quad (4)$$

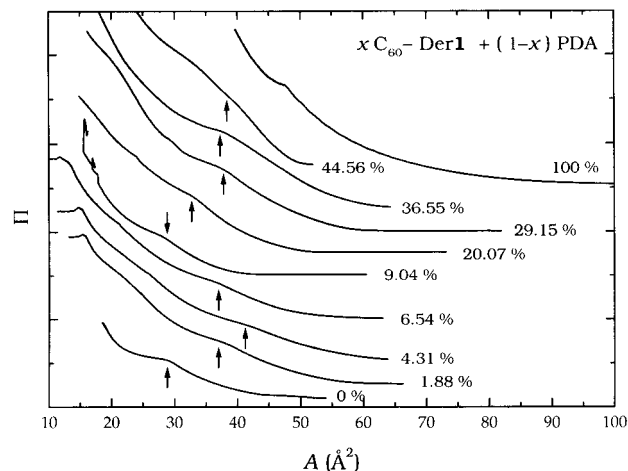


Figure 8. Π - A experimental isotherms of the mixed films of derivative **5** with PDA spread on an aqueous subphase acidified at $\text{pH} = 2$ and at 298 K. The figures near each isotherm refer to the molar fraction of fullerene derivative in the blend. For the sake of clarity, each isotherm has been shifted 5 mN/m upward with respect to the previous one.

This interaction energy is close to zero on the PDA side ($x < 0.2$), thus suggesting an ideal miscibility behavior (supported by the previous observations on the subsistence of pure PDA-like characters in these blends). However, it becomes strongly negative, $\Delta G^E \sim -3k_B T$, for the inhomogeneous blends richer in C_{60} . This energy is significantly higher in absolute value than those reported in the literature for compatible mixtures of fatty compounds,³² $\Delta G^E \sim 0.5k_B T$, but much smaller than the aggregation energy in the film of pure C_{60} , $\Delta G^{\text{agg}} \sim -9k_B T$. The later has been estimated from the difference between the experimental isotherm reported here (see Figure 2) and the theoretical one obtained from a hard sphere model with excluded area, $\sigma = 87 \text{ \AA}^2$ ($\Pi = 0$ at $A > \sigma$, and $\Pi \sim 72$ at $A < \sigma$); a similar value was reported by Obeng and Bard. It is also in quantitative agreement with the value found for clustering in organic solution.³⁷ This high value of ΔG^E should account for the strong π - π cohesive interactions between C_{60} molecules in the film. However, the energy should be considerably reduced when each of them is surrounded by at least half a dozen molecules of the good film-forming agent ($x < 0.2$). A similar conclusion was obtained by Ravaine et al.¹⁴ for other mixed films of fullerene derivatives. The miscibility in this composition range is also supported by the temperature dependence of the isotherms: more compressed isotherms are obtained when T is lowered; a 4.3% decrease in A_0 is found for a blend with $x = 0.0476$ between 25 and 5 °C, and by about 13% for the $x \sim 0.1$ blend. This behavior is at odds with that observed in monolayers of pure fatty acids, where the molecular area characteristic of the LC phase is almost independent of T .^{31,32} Also, at $T \sim 5 \text{ }^\circ\text{C}$ the Π - A isotherms become monotonic: no transitional plateaus are now observed, as occurs for pure PDA at the same temperature,³¹ i.e., the system goes directly from a gaslike phase to a LC phase. If the PDA + C_{60} system is intrinsically incompatible in this composition range ($x < 0.2$), mixing interactions would not play any role in phase behavior, and as a consequence, the limiting area should be independent of T , contrarily to the experimental observation. This might be considered as indirect evidence for quasi-ideal miscibility (weak interactions) in the richer-PDA side of the phase diagram.

PDA + Compound 5. Figure 8 shows the isotherms for the films of the $x\mathbf{5} + (1-x)\text{PDA}$ blend, x being the

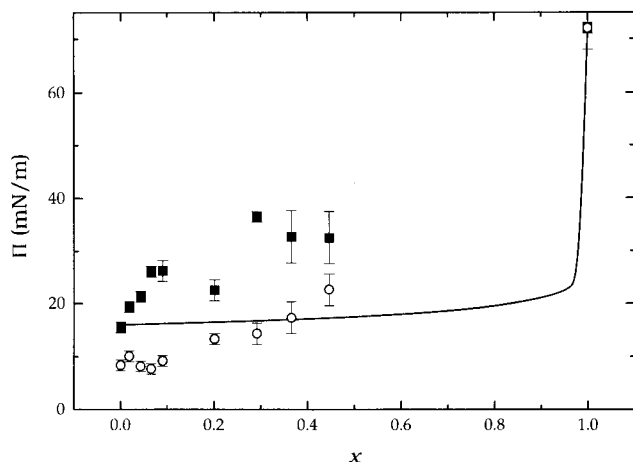


Figure 9. Equilibrium surface pressures of the $x5 + (1-x)$ -PDA blend: (■) at the beginning of the LE/LC transition plateau and (○) at collapse. The continuous line represents the x dependence of the collapse pressure calculated by assuming the ideal behavior described by eq 3.

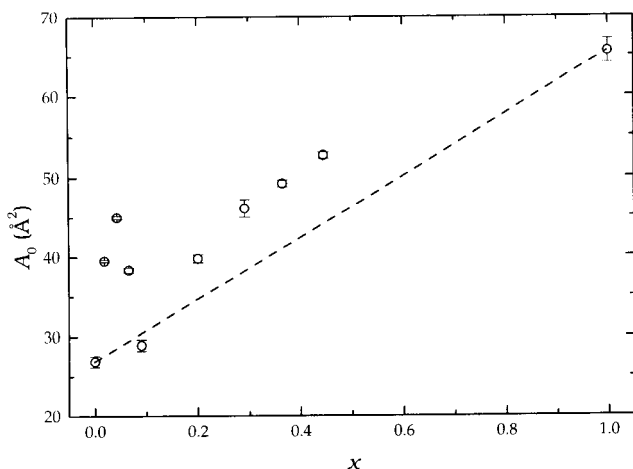


Figure 10. Limiting areas of the isotherms of spread films of the $x5 + (1-x)$ -PDA blend. The continuous line accounts for the ideal-like behavior of the mixing limiting areas, i.e., $A_0^{\text{ideal}} = x5 + (1-x)A_{\text{PDA}}$.

molar fraction of the fullerene derivative. Contrary to the case of pure C_{60} blends, all these isotherms, with the exception of $x = 1.0$, show clearly a curvature change at moderate surface pressures ($\Pi \sim 10\text{--}15$ mN/m), reminiscent of the LE/LC plateau in the pure PDA monolayer. It appears, however, to be more visible in the $x < 0.15$ composition range. As already mentioned for the blend of pure $C_{60} + \text{PDA}$, in this composition regime a true microscopically mixed LC phase exists. A fullerene molecule might stay at the center of the hexagonal arrangement at sufficiently high surface pressures. Figure 9 shows the values of Π at the transition pressure, Π_T , monotonically increase from $\Pi_T \sim 8.5$ mN/m (pure PDA) to higher values as the blends become richer in C_{60} . A similar increase is also observed in the collapse pressure. The x dependence of both characteristic points of the isotherms are thus at odds with the immiscible-like behavior found for the pure $C_{60} + \text{PDA}$ blend. However, there is no quantitative agreement with the theoretical variation predicted from eq 3 by assuming ideal behavior (activity coefficients: $a_1 = a_2 = 1$). The limiting areas (see Figure 10) show an expansion similar to that observed for the previous blend. In the $x < 0.2$ regime, the dimensions of the ordered arrangement in the condensed phase clearly depart from the ideal-mixing behavior, characteristic of

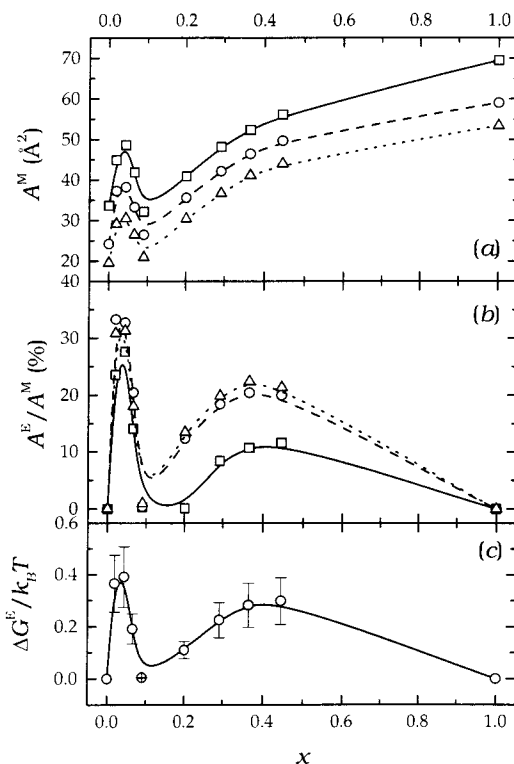


Figure 11. Mixing area A^M (a), excess area A^E (b), and excess Gibbs energy ΔG^E (c) for mixed monolayers of $x5 + (1-x)$ -PDA. Lines are a guide for the eyes. Symbols represent data for different states of the monolayers (in \AA^2 per molecule): (□) 200; (○) 150; (△) 100.

immiscible films. Figure 11a shows the mixing areas at constant values of Π . For the present blend $A^E > 0$ in the whole composition range, in contrast with the results found for that one with pure C_{60} , which exhibits $A^E < 0$ for $x > 0.15$, due to fullerene aggregation in the film. Two composition regimes can be distinguished in Figure 11: (I) the PDA-richer side, $x < 0.15$, characterized by large fractional excess areas, A^E/A^M (up to 32%), and moderately large and positive excess free energy, $\Delta G^E \sim 0.4 k_B T \sim 800$ J mol^{-1} ; (II) a regular disordered quasi-ideal mixture at $x > 0.15$. The differences between both regimes are more clearly understood when correlating the relative width of the LE/LC transition, $s = 2(A_{LE} - A_{LC})/(A_{LE} + A_{LC})$, with an interaction parameter α , defined as follows:^{32,36,38}

$$\alpha = \frac{\Delta G^E}{RT[x(1-x)^2 + x^2(1-x)]} \quad (5)$$

Figure 12 points out that the interaction parameter is maximum in the PDA-rich region I, coinciding with a large value of s , which is a measure of the order parameter for the LE/LC transition of the system. However, as the film becomes richer in fullerene derivative, the PDA character is progressively lost, and the system becomes more disordered; s strongly decreases reaching a near-zero value for the value of x for which the LE/LC transition is also lost.

Since positive values of ΔG^E suggest phase separation in the monolayer,^{32,38} we could speculate about the role of the excluded volume repulsive interactions in forming the mixed films. In region I the PDA molecules are still able to maintain the hexagonal order, and thus a LE/LC

(38) Dynarowicz-Latka, P.; Kita, K. *Adv. Colloid Interface Sci.* **1999**, *79*, 1.

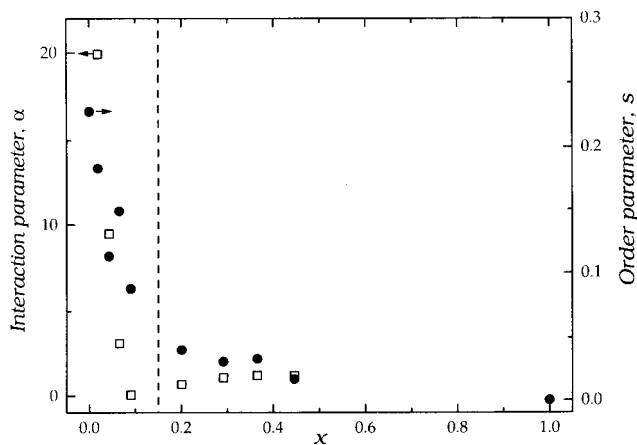


Figure 12. Interaction parameter α (eq 5) and order parameter s for the LE-LC transition in mixed monolayers of $x\mathbf{5} + (1-x)\text{PDA}$.

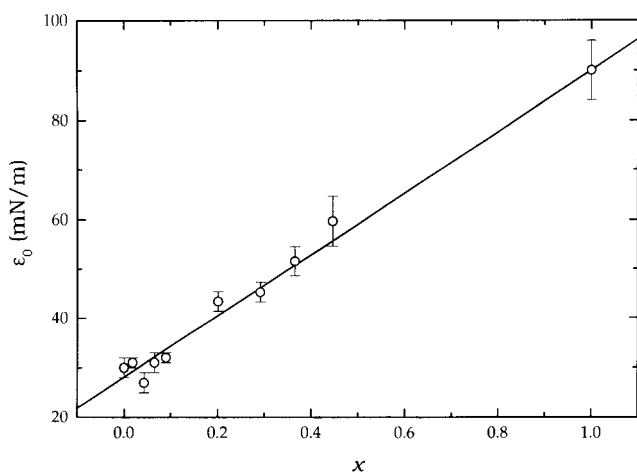


Figure 13. Maximum equilibrium elasticity for $x\mathbf{5} + (1-x)\text{PDA}$. The line is an aid to the eye.

transition is possible: in the LC phase each molecule of fullerene derivative is surrounded by six PDA molecules, thus preventing aggregation between the highly hydrophobic molecules of the C_{60} derivative. However, in region II the PDA molecules act as a kind of point defect for the solidlike arrangement of fullerene spheres; as a consequence, these monolayers are not able to present LE/LC phase transition and are more expanded than that of pure compound **5**.

Figure 13 shows that the maximum value of the compression modulus ϵ_0 increases linearly from a value near to 30 mN/m, corresponding to pure PDA, to a value ca. 90 mN/m for the pure monolayer of the fullerene derivative (**5**). This means that a quasi-continuum medium of weakly interacting fullerene spheres is less deformable in compressing than that one made of PDA molecules strongly anchored at the air-water interface.

3.b. Interfacial Rheology. The rheological properties of monolayers of fullerene derivatives remain unexplored from the experimental point of view. As already mentioned SQELS is a well-suited nonperturbing technique for studying the elasticity ϵ and dilational viscosity κ of interfacial films.²⁰ Moreover, as it can be easily concluded from Figures 2 and 3, for the monolayers of compound **10**, the ratio $\alpha = \epsilon/\gamma$ (ϵ taken as ϵ_0 , and $\gamma = \gamma_0 - \Pi$, with γ_0 the surface tension of pure water) remains below 0.3 for surface areas $A > \sigma$. This ensures a good hydrodynamic coupling between the capillary and the dilational modes^{20,24}

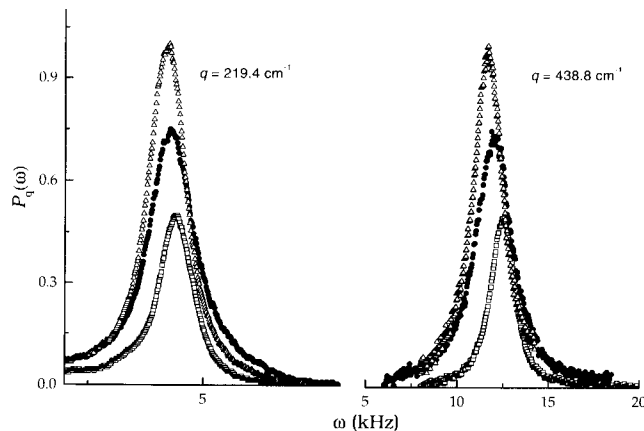


Figure 14. Spectra of scattered light for two values of the wavevector q and three surface states of the compound **10** monolayers: (\square) pure water; (\bullet) $A \approx 200 \text{ \AA}^2$; (\triangle) $A \approx \sigma \approx 89 \text{ \AA}^2$.

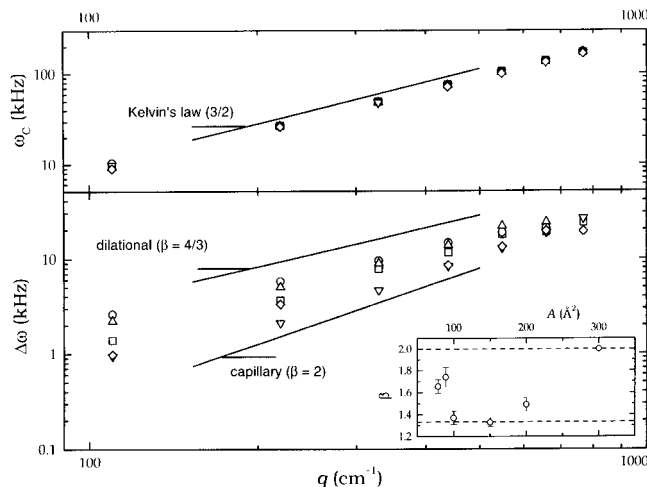


Figure 15. Wavevector dependence of the frequency ω_c and the width at half-height $\Delta\omega_c$ of the spectra of scattered light by the monolayers of compound **10**. The lines represent the limiting laws of Kelvin and the behavior of $\Delta\omega_c$ for pure capillary and dilational waves. The inset shows the exponent of the law $\Delta\omega_c \approx q^\beta$. Symbols are experimental data for different monolayers areas (in \AA^2 per molecule): (\square) 200; (\circ) 150; (\triangle) 100; (∇) 89; (\diamond) 78.

and hence a reasonable sensitivity to the viscoelastic modulus of the dilational mode $\tilde{\epsilon}(\omega) = \epsilon(\omega) + i\omega\kappa(\omega)$.

We have recorded SQELS spectra for seven wavevectors, q , between 100 and 800 cm^{-1} and for surface densities ranging from the high-dilution regime at $\Pi \sim 0$ (200 \AA^2 per fullerene molecule) to highly concentrated states, $A \leq 90 \text{ \AA}^2$, just before the collapse that leads to 3D aggregates. For the sake of example, Figure 14 shows the spectra for two wavevectors and for three different surface states: (i) the free surface of water, (ii) a near half-filled monolayer at $A = 200 \text{ \AA}^2 \sim 2\sigma$, and (iii) a closest-packed monolayer at $A = 89 \text{ \AA}^2 \sim \sigma$.

A first qualitative discussion of the dispersion behavior of the capillary modes can be done fitting the spectra to a Voigt profile, accounting properly for instrumental broadening. Figure 15 shows the q dependence of the propagation frequency ω_c and damping coefficient $\Delta\omega$. In all the cases studied we find $\omega_c^2 \sim (\gamma/q)q^3$ (Kelvin-like dispersion), while a more ambiguous dispersion behavior is observed for the damping of the surface mode. In effect, although $\Delta\omega \sim q^\beta$ is obeyed, the inset of Figure 15b shows that β changes from $\beta \approx 2$ (pure capillary mode behavior)²⁰ for low-density monolayers, to $\beta \approx 4/3$ (pure dilational

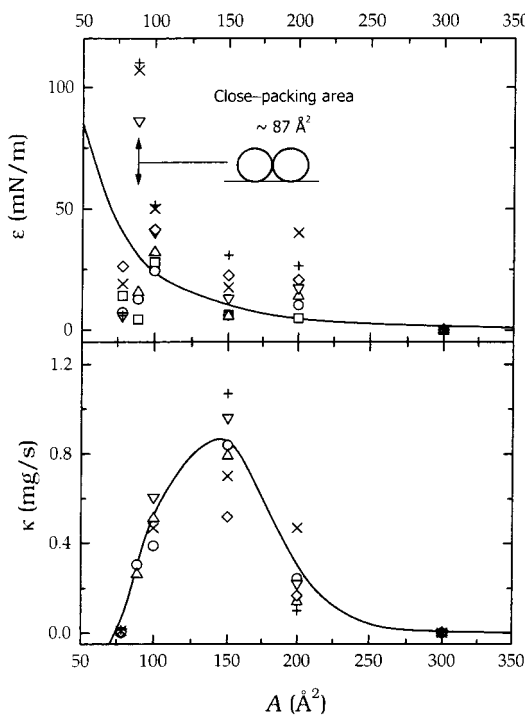


Figure 16. Area dependence (a) of the dynamic elasticity ϵ and (b) of the dilational viscosity κ for the monolayer of compound **10**. Symbols are experimental data for different values of the wavevector q (in cm^{-1}): (\square) 109.7; (\circ) 219.4; (\triangle) 329.1; (∇) 438.8; (\diamond) 548.5; ($+$) 658.2; (\times) 767.9. The continuous line in (a) reproduces the equilibrium compression modulus in Figure 3, calculated from the Π - A isotherm. The line in (b) is only a guide for the eye.

mode behavior) for $A \sim \sigma$, where the fullerene molecules contact each other. For $A < \sigma$ the pure capillary behavior is recovered. This is due in part to the lack of sensitivity of the SQELS technique to the dilational mode (ϵ/γ increases for low areas per molecule) and also to the fact that both ϵ and κ become small for low A values in the frequency range explored in this work (see below).

Figures 16 and 17 show the surface area and the frequency dependencies of ϵ and κ . For the true monolayer states ($A \geq \sigma$) and for low frequencies ($q = 109.7 \text{ cm}^{-1}$) we find $\epsilon \approx \epsilon_0$. This means that a surface disturbance characterized by $q \leq 100 \text{ cm}^{-1}$ (spatial range $\lambda \geq 100 \mu\text{m}$) is well above the Newtonian limit. For such a value of λ a large number of molecules [$O(10^5)$] is involved, and such a collective behaves as a compressible continuum medium which reacts almost instantaneously against a compression (Voigt-like behavior). Still for these expanded states, when q increases above 200 cm^{-1} (λ becomes smaller), ϵ increases with frequency. This means that the monolayer has viscoelastic character. Although the frequency dependence of κ remains doubtful due to its large uncertainty, it is clear that κ grows from near zero values for diluted states, to a maximum $\kappa_{\text{max}} \approx 10^{-3} \text{ mg s}^{-1}$ for $A \approx 150 \text{\AA}^2$. This value of κ_{max} is larger than those found for small amphiphiles^{19,33} or polymers.^{22,24} For condensed states ($A \leq 100 \text{\AA}^2$) we obtain $\epsilon < \epsilon_0$ and κ tends to zero again. This tendency of κ seems similar to the results of the group of Israelachvili who reported very small kinetic shearing viscosities for high-density monolayers of C_{60} confined between two smooth solid walls.^{19,20}

It is possible to make a qualitative link of the previous results with Evans' model for monolayers of C_{60} onto water.¹³ The model is based on the weakly attracting

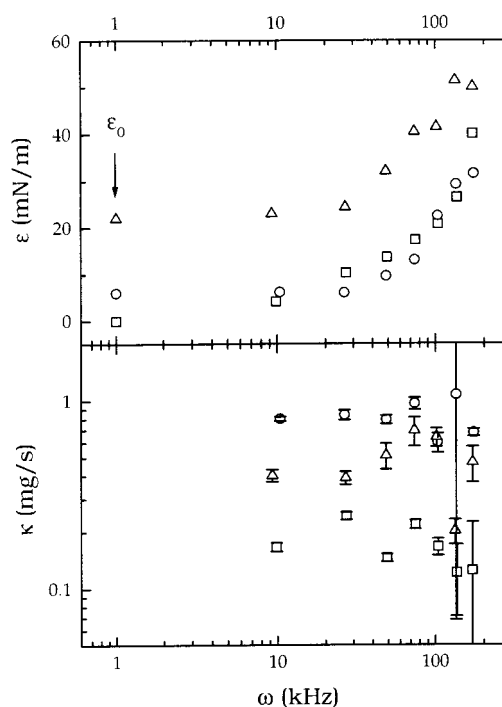


Figure 17. Frequency dependence of the dynamic elasticity ϵ and of the dilational viscosity κ for the monolayers of compound **10**. The values of ϵ plotted at 1 kHz represent the equilibrium value ϵ_0 . Symbols represent experimental data for different states of the monolayer (in \AA^2 per molecule): (\square) 200; (\circ) 150; (\triangle) 100.

Grifalco's pair potential for the C_{60} - C_{60} interaction³⁹ and considers that the frictional force and the random force (thermal agitation) are strong compared to the conservative one (from C_{60} - C_{60} and C_{60} -water interactions).

According to the model, the fullerene molecules are in Brownian motion when lying in contact with the water in the subphase, while they oscillate within the potential well when they are not in contact with the liquid and friction is not present.¹³ According to this picture, the solution of the mass transport equation for the sinusoidal concentration mode induced by surface motion is a pure-longitudinal diffusive mode. As a consequence, the viscoelastic relaxation of the compression stresses must be Maxwell-like in nature⁴⁰

$$\tilde{\epsilon}(\omega) = -A \frac{\delta \Pi}{\delta A} = \frac{\delta \Pi(\omega)}{\delta \ln \Gamma(\omega)} = \epsilon_0 + \epsilon_1 \frac{i\omega\tau}{1 - i\omega\tau} = \epsilon + i\omega\kappa \quad (6)$$

with relaxation time τ and where ϵ_1 accounts for a viscoelastic amplitude related to the Newtonian limit of the dilational viscosity, $\epsilon_1 \equiv \kappa/\tau$. According to this, the diffusion relaxation time can be calculated through

$$\tau = \frac{\epsilon(\omega) - \epsilon_0}{\omega^2 \kappa} \quad (7)$$

This leads to values ranging from $20 \mu\text{s}$ for the near half-filled monolayer ($A = 200 \text{\AA}^2$) to ca. $10 \mu\text{s}$ for more condensed states ($A = 150 \text{\AA}^2 \sim \sigma$). These values are of the same order of the relaxation time calculated by Evans for the diffusive escape of a molecule of C_{60} on top of water, $\tau_D \approx 1 \mu\text{s}$.¹³ Values of $\tau > \tau_D$ seem reasonable for compound

(39) Grifalco, L. A. *J. Phys. Chem.* **1992**, *96*, 858.

(40) Landau, L. D.; Lifshitz, E. M. *The Theory of Elasticity*; Pergamon: Oxford, 1986.

10 due to its higher hydrophilic character, which must lead to a larger viscous drag.

$A \sim 150 \text{ \AA}^2$ corresponds to the equilibrium distance of the Grifalco potential (occurring when the centers of two molecules are 10.1 Å or 1.41 diameters apart).¹³ In the minimum of the potential (steric repulsion balanced with hydrophobic attraction) the energy is much larger than $k_B T$, the system offers a strong resistance to be deformed, and therefore a high shear force is needed to initiate sliding. When the fullerene molecules are compressed further, entering the sharp repulsive branch of the pair potential, the longitudinal stress (shear + compression) needed to initiate motion becomes much lower since they are already thermally activated well above their potential minimum. As a consequence, the dilational parameters, $\epsilon(\omega)$ and κ , both accounting for the longitudinal stresses upon uniaxial compression of the monolayer, strongly decreases (to a near-zero value in the case of κ) as the volume excluded repulsive interaction dominates.

Israelachvili's group related the low viscosities of dense C_{60} systems to the possibility of energy dissipation through the almost free in-plane rotation of the fullerene molecules. The above picture for $A \leq \sigma$ would be compatible with Israelachvili's explanation if the exceeding energy allocated when uniaxially compressing is dissipated through rotation of the fullerene molecules. This is a situation similar to the one found in the shearing-free superliquid (LS) rotator phase fatty acid monolayers.^{41,42} The LS phase also shows a minimum in ϵ and $\omega\kappa$.^{43,44}

(41) Copeland, L. E.; Harkins, W. D.; Boyd, G. E. *J. Chem. Phys.* **1942**, *10*, 357.

(42) Abraham, B. M.; Miyano, K.; Ketterson, J. B.; Xu, S. Q. *Phys. Rev. Lett.* **1983**, *51*, 1975.

(43) Byrne, D.; Earnshaw, J. C. *J. Phys. D* **1979**, *12*, 1145.

(44) Giermanska-Kahn, J.; Monroy, F.; Langevin, D. *Phys. Rev. E* **1999**, *60*, 7163.

4. Conclusions

Three fullerene derivatives have been synthesized. Only when the substituent is a long carbon chain (12 C atoms in compound **10**) does the molecule have enough amphiphilic character to form true Langmuir monolayers. Mixed monolayers of (1 - x)pentadecanoic acid (PDA) + x fullerene derivative have been studied. The Π - A isotherms show that stable monolayers are formed up to high values of x . It has also been found that the LE to LC phase transition characteristic of the PDA monolayers is preserved up to values of x such that the molar ratio PDA/fullerene is 6:1. This has been interpreted in terms of the ability of the PDA molecules to maintain the hexagonal symmetry in the mixed monolayers.

The viscoelasticity of the monolayers of compound **10** has been studied by the analysis of the spectra of light scattered by thermal capillary waves. Two regions can be distinguished: for low-density monolayers ($A \geq 150 \text{ \AA}^2$) the elasticity ϵ and the dilational viscosity κ increase as A decreases. In this region the monolayers have a definite viscoelastic character. For condensed monolayers ($A < 100 \text{ \AA}^2$) ϵ is much smaller than the equilibrium elasticity, and κ tends to zero. This behavior has been explained qualitatively in terms of the model recently proposed by Evans for monolayers of C_{60} .¹³

Acknowledgment. This work was supported in part by Fundación Ramón Areces and by DGEs under Grants PB96-609 and PB98-0818. F. Monroy acknowledges MEC for financial support under a RDT contract.

Supporting Information Available: Experimental ¹³C NMR and high-resolution H NMR spectra of the three new fullerene derivatives synthesized in this work. This material is available free of charge via the Internet at <http://pubs.acs.org>.

LA001479B